The Circular Variance as a Visual Summary of Synchronized Voltage Angle Measurements

Jim Follum, Sinan Aksoy, Sraddhanjoli Bhadra, John Buckheit,
Nick Betzsold, Tianzhixi (Tim) Yin, and Tamara Becejac
Pacific Northwest National Laboratory
james.follum@pnnl.gov

Abstract

Phasor measurement units (PMUs) allow voltage angle differences across power grids to be monitored to identify sudden shifts associated with system disturbances. The Eastern Interconnection Situational Awareness and Monitoring System (ESAMS) was developed to identify such wide-area disturbances and summarize them in reports released the following day. Demonstration of ESAMS in North America's Eastern Interconnection revealed the need for an effective visual summary of the disturbance's impact on voltage angle pairs. This paper proposes the use of the circular variance, a measure of dispersion applicable to angular data, for this purpose. Results based on PMU data from North America's Eastern and Western interconnections indicate that the circular variance provides useful summaries of wide-area voltage angle measurements. They also show that the circular variance may have potential uses when applied to historical data to identify unusual grid conditions.

1. Introduction

Phasor measurement units (PMUs) provide power system operators with a wide-area view of the grid that leads to improved situational awareness and system reliability. The history, applications, and widespread adoption of PMUs throughout the world are discussed in [1]. PMUs typically report voltage phasors (magnitude and phase), current phasors, frequency, and rate of change of frequency (ROCOF) 30 or 60 times per second in 60 Hz systems. These measurements are termed *synchrophasors* because they are time-synchronized across geographically dispersed devices, often using the global positioning system (GPS). The high reporting rate, availability of angle values, and synchronization of PMU measurements make them instrumental in a number of power system applications, including post-mortem analysis, model validation, state estimation, protection, and control [1].

It is now relatively common for system operators to deploy these applications using PMUs from within their own footprint. As these organizations have achieved success, interest has grown in interconnection-scale applications to provide visibility beyond an operating entity's footprint. This interest led to the development of the Eastern Interconnection Situational Awareness and Monitoring System (ESAMS) to foster review and discussion of grid disturbances [2, 3, 4]. Using synchrophasor measurements streamed from across North America's Eastern Interconnection (EI), ESAMS monitors for disturbances such as oscillations, generator trips, and sudden shifts in voltage angle pairs spanning the interconnection. During the system's testing at PJM Interconnection from June 2021 through March 2022, disturbances were summarized in a daily report that was delivered to seven operating entities by email. Events of particular interest were then reviewed and discussed in detail. The work presented in this paper was motivated by the need for a visual summary of a disturbance's impact on voltage angles for use in future versions of the daily report.

The inclusion of voltage angle pair monitoring in ESAMS was motivated by their existing use for a variety of applications. For example, voltage angle pairs can be monitored following a transmission line outage to ensure that synchrocheck relay settings will not prevent the line from returning to service [5]. For corridors containing multiple transmission lines, the phase angle difference across the corridor can provide useful information about stress that may not be apparent in power flows [6]. This concept can be extended to evaluate the stress of an area with boundaries monitored by PMUs [7, 8, 9]. Voltage angle pairs can also serve as a stress indicator at the interconnection-scale [10]. These uses are supported by real-world observations of diverging voltage angle pairs leading up to significant

The Pacific Northwest National Laboratory is operated for the U.S. Department of Energy by Battelle Memorial Institute under Contract DE-AC05-76RL01830. This work was funded by the U.S. DOE.

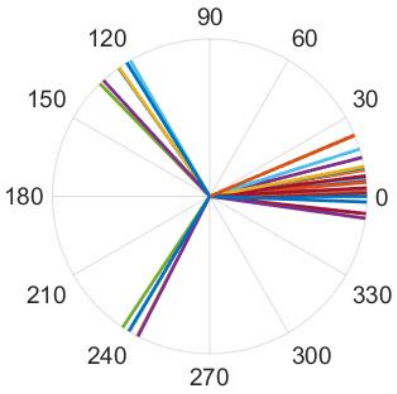

Figure 1. Polar plot of voltage angles corresponding to time 0 in Figure 2.

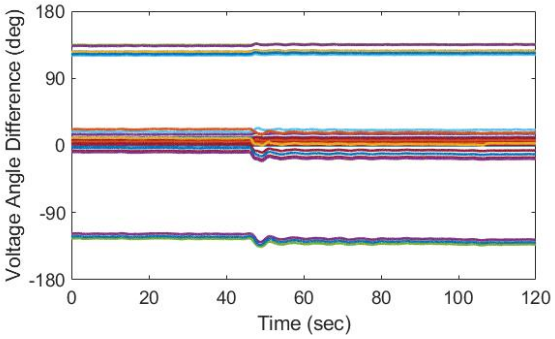

Figure 2. Voltage angle di erences across the EI during a typical system disturbance.

outages [11]. Descriptions of tools used by system operators that monitor voltage angle pairs can be found in [5, 10, 12, 13].

For use in real-time operations, stress and stability monitoring based on phase angle differences requires detailed model-based studies [11]. ESAMS operates exclusively on PMU measurements, with no access to a power system model, Energy Management System (EMS), or Supervisory Control And Data Acquisition (SCADA) measurements. With these constraints, it is not possible to set alarm thresholds like those used in a control room. Rather, ESAMS uses measurements to establish baseline behavior and then identify statistically significant deviations from the baseline [2, 3]. When considering voltage angle pairs, deviations can correspond to changes in topology and generation dispatch. Determining whether these deviations correspond to increases in system stress or decreases in stability margins is beyond the scope of ESAMS. Rather, the system identifies periods of interest to foster discussion and further analysis among the system operators that receive daily reports.

One of the challenges in generating ESAMS reports has been effectively visualizing the impact of a grid disturbance on voltage angle pairs. Polar plots like the one in Figure 1, which are commonly used in real-time monitoring software [14], only display a snapshot of the voltage angles at a particular moment. For static reports, like those generated by ESAMS, a time-domain representation is needed. However, plots containing several voltage angle pairs together, as in Figure 2, tend to be cluttered and difficult to interpret.

This paper describes how the circular variance was selected as a metric to visually summarize the impacts of grid disturbances on voltage angle pairs. As described in Section 2, the circular variance provides an indication of a dataset's spread. Unlike alternative metrics such as the conventional standard deviation, the circular variance is specifically applicable to angular data and therefore provides consistent summaries of the power system's voltage angles during disturbances. Shortcomings of the standard deviation are further discussed in Section 3. The value of the circular variance for summarizing grid disturbances is established in Section 4 using field-measured data from North America's Eastern and Western interconnections. It is also shown that the circular variance has a daily cycle corresponding to load changes. Thus, it may be useful for establishing baseline behavior and identifying deviations during analysis of archived PMU data. The paper concludes with a discussion of findings and expectations for future work in Section 5.

2. Circular Variance

Circular statistics summarize angular data much in the same way that the mean, standard deviation, and variance provide summaries of linear data. To motivate the need for circular statistics, consider the mean of 356 and 2 . Though near each other on the unit circle, their linear mean is far away at 179 . Circular statistics address this type of challenge. Detailed derivations and discussion of circular statistics can be found in [15]. Here, an intuitive introduction to the circular mean and circular variance is provided using an approach and notation from [16].

To analyze angular data, it is helpful to associate each angle, θ_p, with a unit vector. The sum of these vectors divided by the number of data points is given by

$$\mu_1 = \frac{1}{n}\sum_{p=1}^{n} e^{j\ p}. \qquad (1)$$

The angle of μ_1 is known as the *mean direction*. The

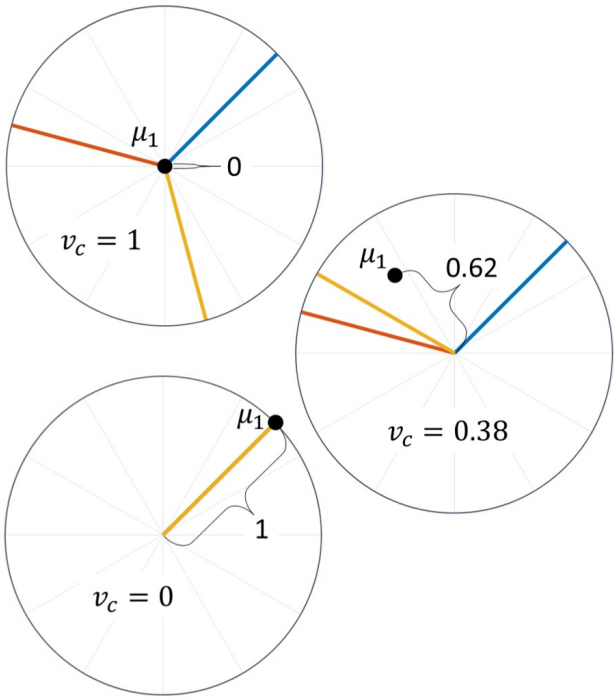

Figure 3. Examples of circular variance for input angles that are evenly distributed (top), equal (bottom) and unevenly distributed (middle).

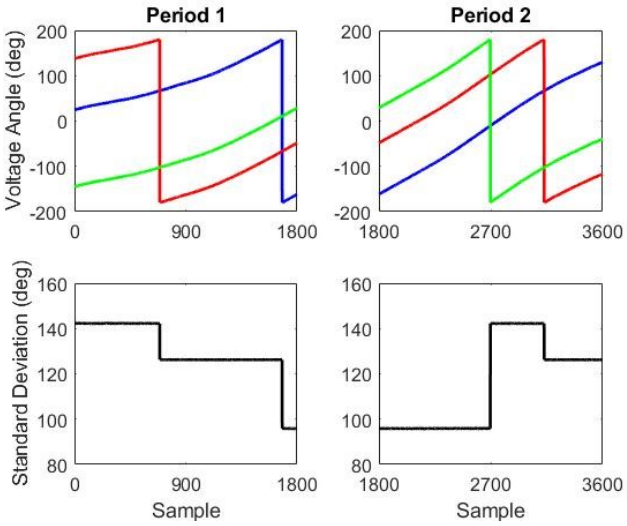

Figure 4. An example of three voltage angles (top) from two adjacent time periods (left and right) with corresponding standard deviations (bottom). The standard deviation shifts every time a voltage angle wraps.

mean direction is useful for summarizing clustered angle values, but it is of less interest in this work because the voltage angles from across an interconnection are not expected to be clustered. Rather, the dispersion of the angles is of primary interest.

The magnitude of μ_1 is related to the dispersion of the data. Consider the three examples in Figure 3. In the top example the input angles are distributed evenly around the unit circle, so $\mu_1 = 0$. The bottom example shows the other extreme, where all three angles are identical. In this case, μ_1 has a magnitude of 1 and its angle is equal to the input data. The middle example shows a case where the input angles are unevenly distributed, leading to an intermediate magnitude of $j\mu_1 j = 0.62$. As dispersion increases, μ_1 moves towards the center of the unit circle and its magnitude decreases. For this reason, the circular variance is defined as

$$v_c = 1 \quad j\mu_1 j. \tag{2}$$

One property of the circular variance that is helpful for displaying results is that its range is between 0 and 1. In addition, its calculation is straightforward and it provides consistent results, regardless of where angles are located on the unit circle. To further motivate its use, shortcomings of the standard deviation for this application are discussed in the following section.

3. Shortcomings of the Linear Standard Deviation

The standard deviation was first considered for this application after seeking a summarizing metric through the application of graph theory. The relationship between graph theory and the standard deviation is not critical to support use of the circular variance, but it is described in the Appendix for the interested reader. This section describes the shortcomings of the standard deviation as a summarizing statistic for voltage angle measurements that led to the use of the circular variance.

The examples in this section are based on a set of 3600 voltage angle measurements from three PMUs. The 3600 samples are split into two periods, with Period 1 covering the first 1800 samples and Period 2 covering the second 1800 samples. The three voltage angle measurements and their corresponding standard deviations are plotted in Figure 4. Note that the standard deviation shifts significantly each time a voltage angle wraps between 180 and 180 . This is undesirable because the shifts are unrelated to changes in the power system's state; they only reflect the way the angles are represented.

It might seem obvious to address this problem by unwrapping the voltage angles to remove jumps between

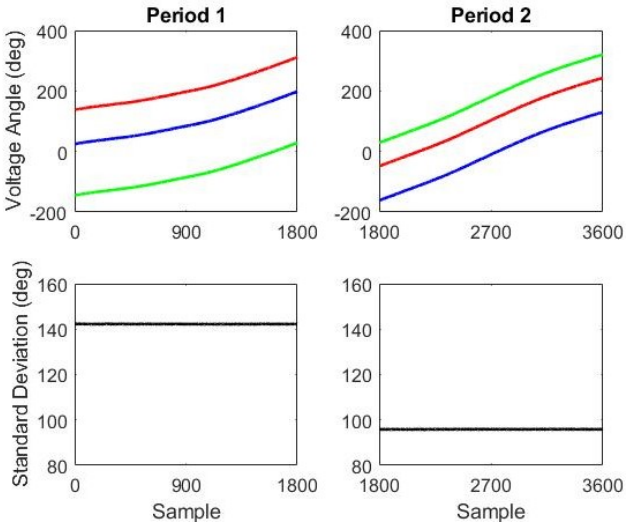

Figure 5. Voltage angles unwrapped across time (top) from two adjacent time periods (left and right) with corresponding standard deviations (bottom). The standard deviations are smooth but do not match between time periods.

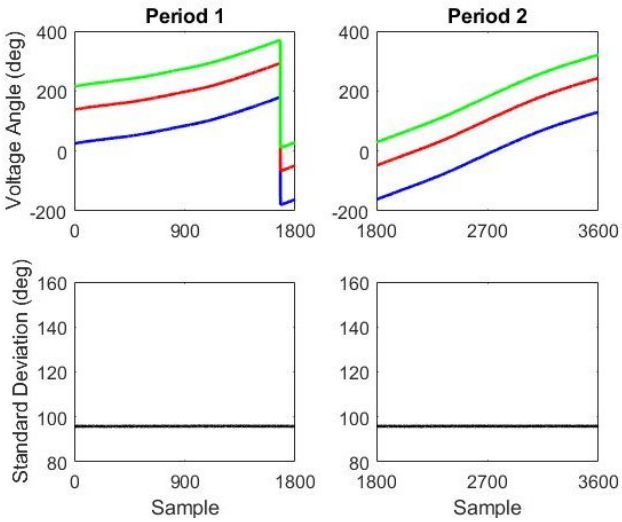

Figure 6. Voltage angles unwrapped across PMUs (top) from two adjacent time periods (left and right) with corresponding standard deviations (bottom). The standard deviations match for both time periods.

180 and 180 . This can be done with a simple command in multiple programming languages. Results with unwrapped voltage angles are presented in Figure 5. Though the sudden shifts in the standard deviation are removed, the values are significantly different between Periods 1 and 2. It is undesirable for a summarizing metric's value to depend on when the analysis begins.

One approach to address this limitation is to unwrap the voltage angles across PMUs. At each time step, the measurement from the red curve is adjusted by 360 if it is more than 180 from the blue curve. Then the measurement from the green curve is adjusted by 360 if it is more than 180 from the red curve. Results from this approach are presented in Figure 6. As desired, the standard deviation is consistent between the two periods. However, this approach is also flawed because it depends on the ordering of the signals. Figure 7 shows that the standard deviations for this approach shift for Period 1 when the signal order changes from *f*blue, red, green*g* to *f*red, blue, green*g*. It is undesirable for a summarizing metric's value to depend on the order that the input data is arranged.

These difficulties motivated the use of the circular variance because it is well suited to angular data. Specifically, it gives consistent results regardless of when the analysis begins or the arrangement of the input data. Its limited range between 0 and 1 is also convenient for interpretation and plotting. The usefulness of the circular variance for summarizing

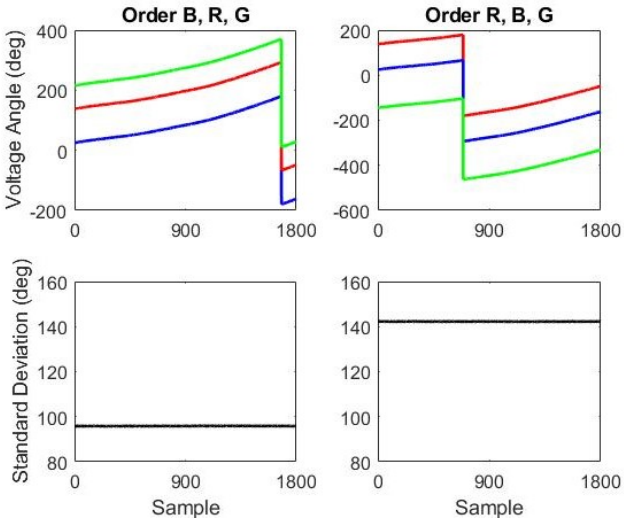

Figure 7. Voltage angles unwrapped across PMUs (top) with corresponding standard deviations (bottom). The standard deviations do not match for signal orders {blue, red, green} (left) and {red, blue, green} (right).

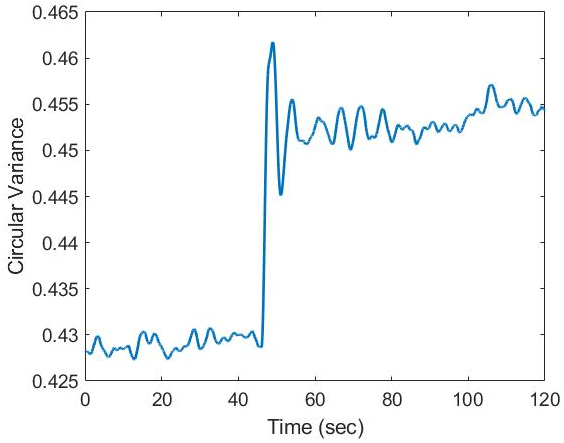

Figure 8. Circular variance of EI voltage angles during the system disturbance in Figure 2.

voltage angle measurements is further established with field-measured data in the following section.

4. Results

In Section 1, Figure 2 was used to motivate the need for a visual summary of a power system's voltage angle differences. The voltage angles used to generate Figures 1 and 2 were collected from the EI during the ESAMS demonstration. They span much of the EI. As a first example of the circular variance's usefulness, consider the summary of these same measurements presented in Figure 8. The circular variance clearly shows that the system disturbance caused the voltage angles to spread apart, which is not easy to see in the multiple voltage angle pairs of Figure 2.

Additional examples of the circular variance making it easier to interpret disturbance recordings are presented in Figures 9 and 10. These figures were also generated using data from the EI collected during the ESAMS demonstration. Figure 9 shows a case where the shift in voltage angles caused by the system disturbance was undone within a few minutes. No such return is observable in Figure 8 or the minutes that followed it. Figure 10 shows a case where the disturbance had a very brief impact on the voltage angles. Together, Figures 8-10 show the diversity of responses to grid disturbances and how the circular variance provides a better visual summary than plots containing several voltage angle differences.

Additional testing was completed with measurements collected by Bonneville Power Administration (BPA), a transmission owner and operator headquartered in Portland, Oregon. Figure 11 depicts the circular variance and voltage angle

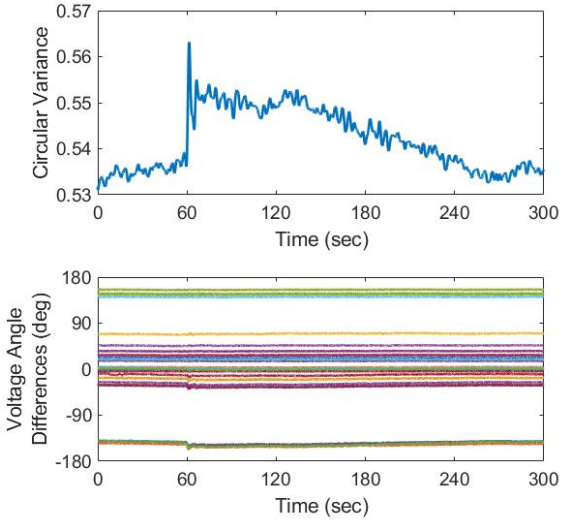

Figure 9. Disturbance of the EI as depicted by the circular variance of voltage angles (top) and a set of voltage angle pairs (bottom).

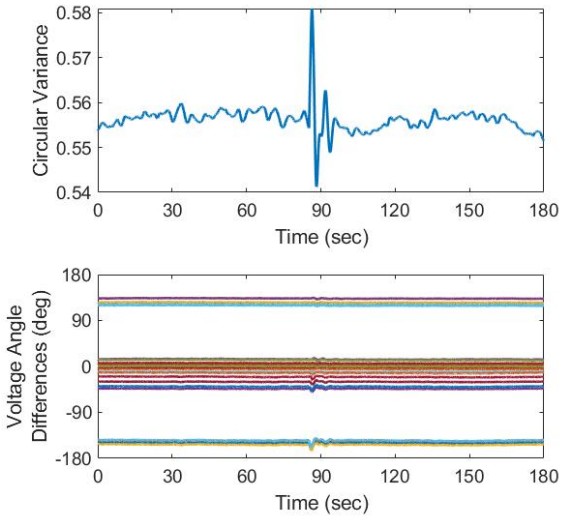

Figure 10. Disturbance of the EI as depicted by the circular variance of voltage angles (top) and a set of voltage angle pairs (bottom).

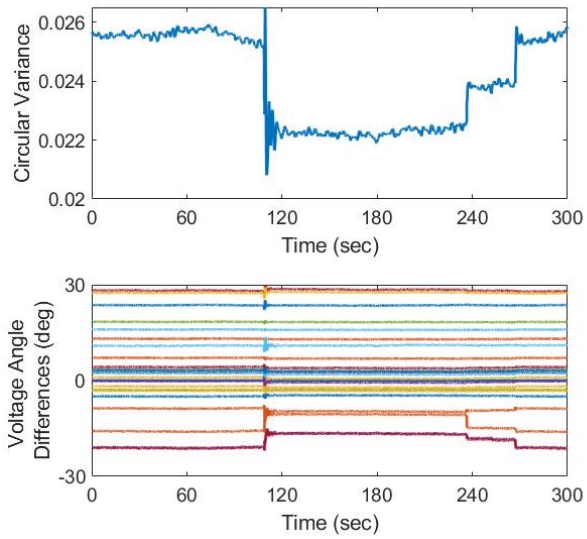

Figure 11. Circular variance (top) and full set of voltage angle pairs (bottom) indicating the outage of transmission lines and their re-energization in two steps.

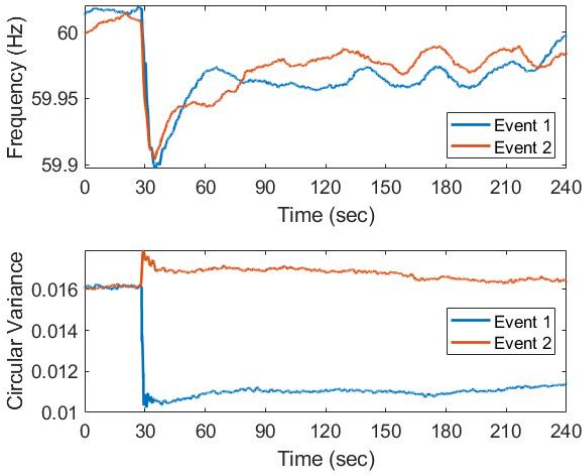

Figure 12. Frequency measurements (top) and circular variance (bottom) for two grid disturbances.

differences for a fault along a major transmission corridor occurring just prior to the 120-second mark in the plots. The resulting line trip caused the spread of voltage angles to decrease for approximately two minutes. The circular variance's return to its initial value approximately 2 minutes later provides strong evidence that the lines were restored in two steps, bringing the system back to its initial state.

Next, consider the two frequency disturbances in Figure 12. These events occurred several days apart, but they appear very similar in the frequency measurements. Though the circular variance starts off at similar values in the two cases, the responses to the disturbances are significantly different. In Event 1, the separation between voltage angles tended to decrease, resulting in a large drop in the circular variance that persisted for the entire period during which the frequency recovered. However, Event 2 led to a small increase that gradually faded as the frequency recovered. In this way, the circular variance provides additional information about the effect of a system disturbance within a particular footprint. The full set of angle pairs displayed in Figure 13 validate the circular variance results. They also demonstrate that such plots tend to be crowded and are not ideal for communicating these insights in ESAMS reports.

Along with evaluating disturbances, the circular variance may be used to establish a baseline and identify unusual periods in historical data archives. To

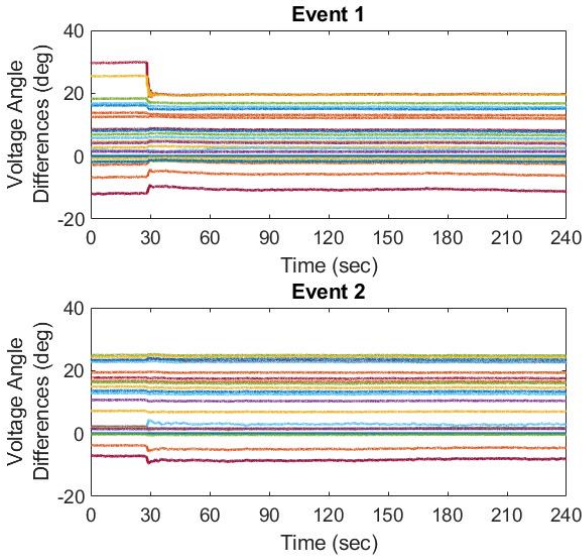

Figure 13. Full set of voltage angle di erences for Event 1 (top) and Event 2 (bottom) of Figure 12.

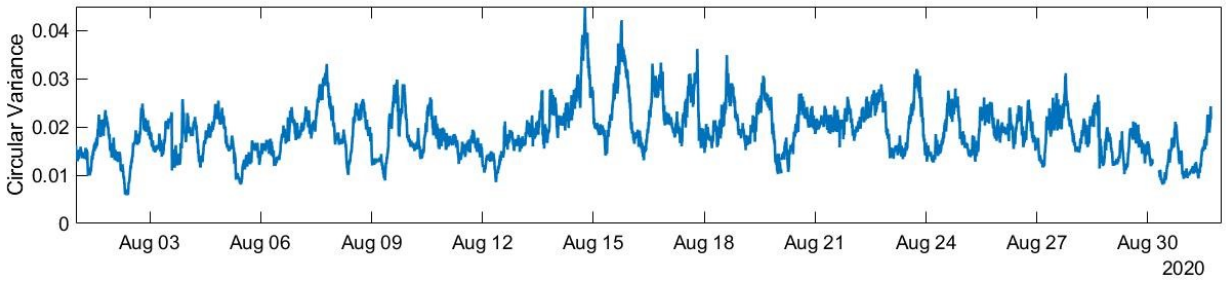

Figure 14. Circular variance of voltage angles from the BPA system for the month of August 2020.

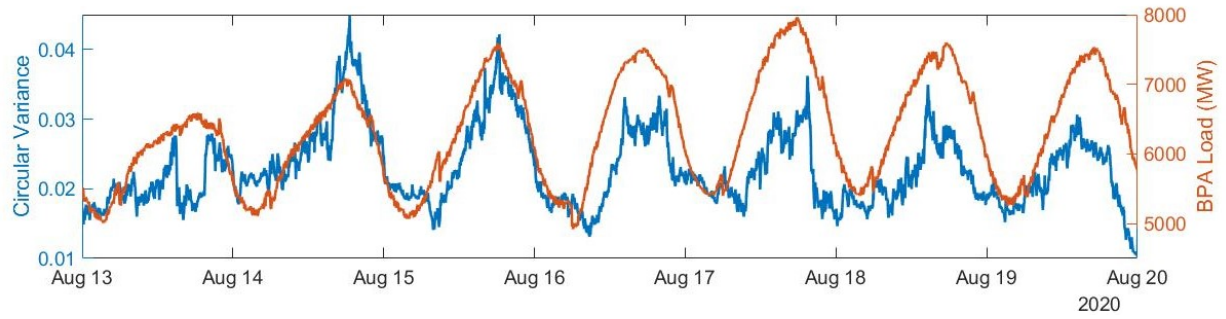

Figure 15. Circular variance of BPA's voltage angles and BPA load for a week in August 2020 with very high loading in the Western US power grid.

demonstrate this, the circular variance was calculated for the entire month of August 2020. The full set of results is presented in Figure 14. The circular variance tends to follow a daily cycle, a pattern that is easier to see for the one-week period in Figure 15. This figure also shows the correlation between the circular variance and the total load reported by BPA as a balancing authority [17]. The week in Figure 15 includes the circular variance's two largest peaks from the month of August. These peaks occurred on the same two days that rolling blackouts were initiated in California to manage an insufficient power supply driven by high temperatures throughout the Western US [18]. It is interesting to note that the higher loads experienced by BPA later in the week were accompanied by lower values for the circular variance. This result is not intended to motivate the circular variance's use to monitor grid stress or generate alarms. Rather, it indicates that the circular variance may serve as a useful metric when searching historical data for periods of interest.

Analyzing such long record lengths requires consideration of data availability. Measurements can be unavailable due to scheduled maintenance, communication dropouts, data quality problems, etc. In the BPA dataset analyzed here, measurements from one PMU were omitted because they were unrealistic for the entire analysis period, likely due to work being performed at the substation. All other periods of data unavailability lasted for less than a few seconds and could be addressed with simple linear interpolation. In general, signals that cannot be interpolated should be removed from the analysis to avoid shifts in the circular variance as the number of input signals changes.

5. Conclusion

The results presented in the previous section demonstrate the utility of the circular variance for summarizing voltage angle measurements. In particular, it can provide valuable insight into a power system's response to disturbances, making it an excellent tool for visualizing the disturbances detected by ESAMS. The circular variance also shows potential when applied to historical data to identify unusual grid conditions. This application requires additional study to formalize methods for determining when the circular variance indicates grid conditions are unusual enough to warrant review.

Another potential avenue for future work is extracting additional practical insight from the circular variance. For example, the signals contributing most to a change in the circular variance during a disturbance could be identified and used to localize the area of the grid most impacted by the disturbance. Further,

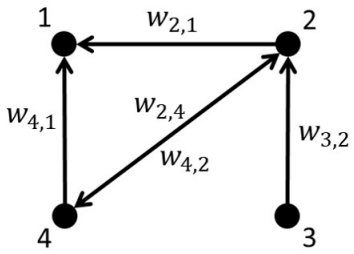

Figure 16. Example of a weighted digraph with four vertices. Edge weights are denoted as $w_{p,q}$.

a sensitivity analysis could be conducted to identify which signals have the greatest impact on the circular variance's value. There may be additional value from combining an interconnection-scale analysis, which was demonstrated with EI data, with a regional analysis like the one performed with BPA data. Studies such as these could be used to extend the value of the circular variance's application to voltage angle measurements beyond a visual summary.

6. Appendix

As mentioned in Section 3, the circular variance was selected after recognizing shortcomings in the standard deviation's application to angular data. The standard deviation came into consideration after attempting to derive a metric through the application of graph theory. This appendix describes that initial effort to better explain why the standard deviation was first considered.

In mathematics, a graph is a representation of relationships between objects. More formally, a graph $G = (V, E)$ consists of a set of objects V called *vertices* and a set of pairs of vertices E called *edges*, which denote relationships. Edges may also be assigned weights, creating a weighted graph, and direction, creating a directed graph (digraph). In this work, we will consider weighted digraphs. Figure 16 illustrates an example of a weighted digraph, where vertices are represented by dots and edges by directed arcs. Letting $p \; ! \; q$ indicate an edge exists from vertex p to vertex q, the edge weights are denoted as w_{pq}. The *adjacency matrix* A defining a weighted digraph is then

$$A_{pq} = \begin{cases} w_{pq} & \text{if } p \; ! \; q, \\ 0 & \text{otherwise.} \end{cases} \tag{3}$$

The need to quantify the similarity between two graphs arises in many domain areas. Accordingly, graph theorists have proposed a plethora of *graph distance* measures, such as graph edit distance [19], iterative vertex-neighborhood methods [20], maximum common subgraph based distance [21], and others. In this work, we utilize a notion of graph distance based on the eigenvalues of the adjacency matrix. Graph eigenvalues, including adjacency, Laplacian, and normalized Laplacian eigenvalues, serve as global summary statistics that capture far-ranging structural properties of the graph [22].

If the graph is undirected, the eigenvalues of the adjacency matrix are real,

$$\lambda_1(A) \quad \lambda_2(A) \quad \lambda_n(A).$$

Then the adjacency spectral distance between graphs with adjacency matrices A_1 and A_2 is defined as [23]

$$D(A_1, A_2) = \sqrt{\sum_{i=1}^{n} j\lambda_i(A_1) \quad \lambda_i(A_2)j^2}. \tag{4}$$

Extending these concepts to digraphs requires care because the eigenvalues may be complex. As will be discussed soon, the particular class of digraph adjacency matrices we study are guaranteed to have precisely two nonzero, purely imaginary eigenvalues of the form

$$\lambda(A_k) = \quad j\omega_k. \tag{5}$$

Consequently, we propose a straightforward analog of spectral distance between these matrices. Plugging (5) into (4) simplifies to

$$D(A_1, A_2) = \sqrt{2}j\omega_1 \quad \omega_2 j. \tag{6}$$

To build the graphs considered in this paper, a vertex was assigned to each PMU. Edges were placed between all PMU pairs, and the difference between the voltage angles for each PMU pair was assigned as the edge's weight. This setup is depicted in Figure 17, where θ_p denotes the voltage angle measurement at PMU p. With these weights, the adjacency matrix becomes

$$A^0_{pq} = \theta_p \quad \theta_q. \tag{7}$$

The ^{0} symbol denotes that this matrix is a special case of (3).

The initial concept for this work was to compare two graphs, one constructed with voltage angles before a grid disturbance and the other constructed after the disturbance. The adjacency spectral distance was selected to quantify this comparison, so the eigenvalues of A^0_{pq} were of interest. In the configuration given by (7), the adjacency matrix has precisely two nonzero eigenvalues, which we show are given by

$$\lambda(A^0) = \quad j\sqrt{n\sum_{p=1}^{n}\theta_p^2 \quad \left(\sum_{p=1}^{n}\theta_p\right)^2}. \tag{8}$$

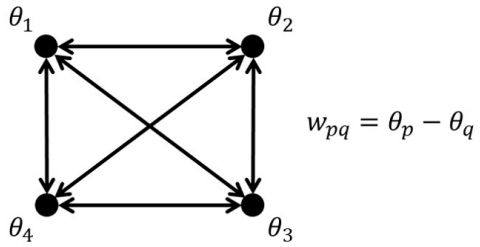

Figure 17. Setup of the graph used to analyze voltage angle measurements, which are denoted as $_p$.

Proof. Letting $\mathbf{\Theta} := (\theta_1, \ldots, \theta_n)$, the matrix A^0 may be written as $\mathbf{\Theta 1}^T \quad \mathbf{1\Theta}^T$, where $\mathbf{1}$ denotes the all-ones vector. Since $\mathbf{\Theta}$ is not a multiple of $\mathbf{1}$, it follows A^0 has rank 2 and has precisely 2 nonzero eigenvalues. Any eigenvector $\mathbf{x}$ of A^0 associated with a nonzero eigenvalue can be written as $\mathbf{x} = c_1\mathbf{\Theta} + c_2\mathbf{1}$, where c_1 and c_2 are nonzero. Rearranging $A^0\mathbf{x} = \lambda\mathbf{x}$, we have

$$(c_1\mathbf{1}^T\mathbf{\Theta} + c_2\mathbf{1}^T\mathbf{1} \quad c_1\lambda)\mathbf{\Theta} + (\quad c_1\mathbf{\Theta}^T\mathbf{\Theta} \quad c_2\mathbf{\Theta}^T\mathbf{1} \quad c_2\lambda)\mathbf{1} = 0.$$

Since $\mathbf{\Theta}$ and $\mathbf{1}$ are linearly independent, the coefficients in the equation above must also be zero, yielding a homogenous linear system

$$\begin{bmatrix} \mathbf{1}^T\mathbf{\Theta} & \lambda & \mathbf{1}^T\mathbf{1} \\ \mathbf{\Theta}^T\mathbf{\Theta} & & \mathbf{\Theta}^T\mathbf{1} \quad \lambda \end{bmatrix},$$

which, upon solving, yields the nonzero eigenvalues of A^0 are $\quad j\sqrt{\mathbf{1}^T\mathbf{1}\mathbf{\Theta}^T\mathbf{\Theta} \quad (\mathbf{\Theta}^T\mathbf{1})^2}$.

□

Letting μ denote the sample mean of $\mathbf{\Theta}$, (8) can be rearranged as

$$\begin{aligned} \lambda(A^0) &= \quad j \quad n\sqrt{\frac{1}{n}\sum_{p=1}^{n}\theta_p^2 \quad \left(\frac{1}{n}\sum_{p=1}^{n}\theta_p\right)^2} \\ &= \quad j \quad n\sqrt{\frac{1}{n}\sum_{p=1}^{n}\theta_p^2 \quad \mu^2} \\ &= \quad j \quad n\sqrt{\frac{1}{n}\sum_{p=1}^{n}(\theta_p \quad \mu)^2} \\ &= \quad jns \end{aligned} \tag{9}$$

where s denotes the uncorrected sample standard deviation of $\mathbf{\Theta}$ (the corrected sample standard deviation, which is more commonly used in practice, is scaled by $n \quad 1$ instead of n).

The fact that only two eigenvalues are nonzero leads to a useful interpretation of the distance between graphs. Let s_1 and s_2 denote the standard deviation terms associated with adjacency matrices A_1^0 and A_2^0, which represent two points in time. Then it follows from (6) that

$$D(A_1^0, A_2^0) = \overline{p}\overline{2n}js_1 \quad s_2j. \tag{10}$$

Thus, the spectral distance between two graphs constructed according to (7) is proportional to the difference between the standard deviations of the angle pairs.

This result can be extended to summarize changes in the power system's voltage angles over time. Rather than calculating (10) for two points in time, the standard deviation can be calculated for every PMU report.

When shortcomings in the standard deviation's application to angular data were identified, it was replaced with an alternative measure of dispersion designed specifically for angular data: the circular variance. From a graph theory perspective, the circular variance is not just a measure of the voltage angles' dispersion. It also indicates how much the power system, represented as a graph defined by (7), changes over time.

Acknowledgment

The authors would like to thank Sandra Jenkins, DOE Office of Electricity, Transmission Reliability and Renewable Integration program, for her support and guidance. We also gratefully acknowledge the many individuals from Eastern Interconnection system operators who have provided support for the ESAMS project. Hamed Golestani, Subbarao Eedupuganti, David Hislop, Christopher Callaghan, and Eric Hsia from PJM deserve special thanks, along with Shaun Murphy, who is formerly with PJM. The authors would also like to thank Bonneville Power Administration (BPA) for providing measurements to support this study. Finally, we thank Joseph Eto from Lawrence Berkeley National Laboratory for leading the ESAMS effort and our collaborators at EPG, Ken Martin, Neeraj, Nayak, Horacio Silva-Saravia, Simon Mo, and Song Xue.

References

[1] A. G. Phadke and T. Bi, "Phasor measurement units, WAMS, and their applications in protection and control of power systems," *Journal of Modern Power Systems and Clean Energy*, vol. 6, no. 4, pp. 619–629, 2018.

[2] B. Amidan, J. Follum, T. Yin, and N. Betzsold, "FY18 Discovery Thru Situational Awareness: Anomalies,

oscillations, and classification," PNNL-27812. Richland, WA: Pacific Northwest National Laboratory., Tech. Rep., 2018.

[3] J. Follum, N. Betzsold, T. Yin, and J. Buckheit, "Event screening methods for the Eastern Interconnection Situational Awareness and Monitoring System (ESAMS)," PNNL-30137. Richland, WA: Pacific Northwest National Laboratory, Tech. Rep., 2020.

[4] J. Follum, T. Yin, and N. Betzsold, "Regional oscillation source localization: Implementation in the ESAMS tool." PNNL-29612. Richland, WA: Pacific Northwest National Laboratory, Tech. Rep., 2020.

[5] "Phase angle monitoring: Industry experience following the 2011 Pacific Southwest outage: Recommendation 27," North American Electric Reliability Corporation (NERC) Synchronized Measurement Subcommittee (SMS), Tech. Rep., 2016. [Online]. Available: https://www.nerc.com/comm/PC/Pages/Synchronized-Measurement-Subcommittee-(SMS)-Scope.aspx

[6] J. Giri, M. Parashar, J. Trehern, and V. Madani, "The situation room: Control center analytics for enhanced situational awareness," *IEEE Power and Energy Magazine*, vol. 10, no. 5, pp. 24–39, 2012.

[7] J. W. Simpson-Porco and N. Monshizadeh, "Model-free wide-area monitoring of power grids via cutset voltages," in *2016 IEEE 55th Conference on Decision and Control (CDC)*, 2016, pp. 7508–7513.

[8] A. Darvishi and I. Dobson, "Threshold-based monitoring of multiple outages with PMU measurements of area angle," *IEEE Transactions on Power Systems*, vol. 31, no. 3, pp. 2116–2124, 2016.

[9] W. Ju, I. Dobson, K. Martin, K. Sun, N. Nayak, I. Singh, H. Silva-Saravia, A. Faris, L. Zhang, and Y. Wang, "Real-time area angle monitoring using synchrophasors: A practical framework and utility deployment," *IEEE Transactions on Smart Grid*, vol. 12, no. 1, pp. 859–870, 2021.

[10] "Using synchrophasor data for phase angle monitoring," North American Synchrophasor Initiative (NASPI) Control Room Solutions Task Team (CRSTT), Tech. Rep., 2016. [Online]. Available: https://www.naspi.org/node/351

[11] "Real-time application of synchrophasors for improving reliability," North American Electric Reliability Corporation (NERC) Real-Time Application of PMUs to Improve Reliability Task Force (RAPIR TF), Tech. Rep., 2016. [Online]. Available: https://www.naspi.org/node/664

[12] D. Kosterev, "Synchrophasor technology at BPA," in *Power Electronics and Power Systems*. Springer International Publishing, may 2018, pp. 77–127.

[13] H. Yuan, H. Zhang, and Y. Lu, "Virtual bus angle for phase angle monitoring and its implementation in the western interconnection," in *2018 IEEE/PES Transmission and Distribution Conference and Exposition (T D)*, 2018, pp. 1–9.

[14] A. Agarwal, J. Balance, B. Bhargava, J. Dyer, K. Martin, and J. Mo, "Real Time Dynamics Monitoring System (RTDMS®) for use with synchrophasor technology in power systems," in *2011 IEEE Power and Energy Society General Meeting*, 2011, pp. 1–8.

[15] N. Fisher, *Statistical Analysis of Circular Data*, ser. Statistical Analysis of Circular Data. Cambridge University Press, 1995. [Online]. Available: https://books.google.com/books?id=wGPj3EoFdJwC

[16] K. Davidson, J. Goldschneider, L. Cazzanti, and J. Pitton, "Feature-based modulation classification using circular statistics," in *IEEE MILCOM 2004. Military Communications Conference, 2004.*, vol. 2, 2004, pp. 765–771 Vol. 2.

[17] Wind generation and total load in the BPA balancing authority. Bonneville Power Administration (BPA). Accessed November 3, 2020. [Online]. Available: https://transmission.bpa.gov/Business/Operations/Wind/default.aspx

[18] "Final root cause analysis: Mid-August 2020 extreme heat wave," Prepared by the California Independent System Operator, California Public Utilities Commission, and California Energy Commission, Tech. Rep., 2021. [Online]. Available: http://www.caiso.com/Documents/Final-Root-Cause-Analysis-Mid-August-2020-Extreme-Heat-Wave.pdf

[19] A. Sanfeliu and K.-S. Fu, "A distance measure between attributed relational graphs for pattern recognition," *IEEE Transactions on Systems, Man, and Cybernetics*, vol. SMC-13, no. 3, pp. 353–362, may 1983.

[20] V. D. Blondel, A. Gajardo, M. Heymans, P. Senellart, and P. V. Dooren, "A measure of similarity between graph vertices: Applications to synonym extraction and web searching," *SIAM Review*, vol. 46, no. 4, pp. 647–666, jan 2004.

[21] M.-L. Fernández and G. Valiente, "A graph distance metric combining maximum common subgraph and minimum common supergraph," *Pattern Recognition Letters*, vol. 22, no. 6-7, pp. 753–758, may 2001.

[22] F. C. Graham, *Spectral graph theory*. American Mathematical Soc., 1997, vol. 92.

[23] I. Jovanović and Z. Stanić, "Spectral distances of graphs," *Linear Algebra and its Applications*, vol. 436, no. 5, pp. 1425–1435, 2012. [Online]. Available: https://www.sciencedirect.com/science/article/pii/S0024379511006021